Influence of nozzle geometry on spray and combustion characteristics related to large two-stroke engine fuel injection systems

Fuel 294 (2021) 120455

Contents lists available at ScienceDirect

Fuel

journal homepage: www.elsevier.com/locate/fuel

Full Length Article

Influence of nozzle geometry on spray and combustion characteristics related to large two-stroke engine fuel injection systems

R. Balz [a,b,*], G. Bernardasci [b], B. von Rotz [b], D. Sedarsky [a]

[a] Chalmers University of Technology, Department of Mechanics and Maritime Sciences, Göteborg, Sweden
[b] Winterthur Gas & Diesel Ltd., Winterthur, Switzerland

ARTICLE INFO

Keywords:
Cavitation
Spray
Marine diesel engine
Fuel injection
Combustion

ABSTRACT

As emission regulations for large two-stroke marine Diesel engines increase as well, the manufacturers face similar problems as small-sized engine builders. The fuel injection, spray formation and subsequent combustion process remain among the main drivers for emissions of direct-injection, compression-ignition internal combustion engines. Since the fuel injection nozzle design of large two-stroke marine Diesel engines differs significantly, not only in size but especially regarding their non-symmetricity and eccentrical orifice arrangement, compared with four-stroke engines, the bulk of research available related to this topic is very limited.

To further deepen the understanding of how in-nozzle cavitation flow during the fuel injection process affects the combustion behaviour in large two-stroke marine Diesel engines, transparent nozzle geometries have been used to link the cavitation phenomena with spray and combustion characteristics. A total of six single-orifice nozzles based on the original five-orifice nozzle design of large two-stroke marine Diesel fuel injectors, with and without hydro-erosive grinding, have been experimentally investigated under realistic engine conditions using highspeed optical measurement techniques and a unique constant-volume spray chamber that geometrically represents a combustion chamber of a large two-stroke marine Diesel engine at top dead centre.

The spray morphology and combustion results reveal significant differences between the non- and hydro-erosive ground nozzle geometries. While the standard and angled nozzle versions remain similar, the eccentrical nozzle with its distinctive in-nozzle swirl cavitation pattern behaves differently, leading to a very reliable start of ignition behaviour and extreme wide spray angle.

1. Introduction

Large two-stroke marine Diesel engines belong to the most efficient internal combustion engines existing and propel commercial marine vessels all over the oceans [1,2]. The engine's two-stroke design, large bore, and uniflow scavenging lead to a single, centrically arranged exhaust valve and a multi-fuel injection arrangement. The nozzles of those fuel injectors are different from centrically placed injectors common in small- and medium-sized engines as found in cars and trucks. Usually two or three fuel injectors are arranged circumferential around the cylinder and the orifices of each nozzle are arranged to inject the fuel into the charged air swirl without contacting the cylinder liner walls. This injector and nozzle layout allows better air/fuel mixture and consequent uniform temperature distribution. As the fuel admission in large two-stroke marine diesel engines is peripherical and the fuel is injected into a high swirling flow field originating from the uniflow-scavenged cylinder design, the nozzle tip layout and its orifice sizes are providing the best suitable mixture formation for a low fuel consumption in combination with low emissions. Furthermore, the design of the nozzle tip is taking into account the limits of component temperatures (e.g. exhaust valve or piston) in the combustion chamber as well as the avoidance of deposits.

However, the nozzle designs with typically five orifices have a rather complicated design with different angles and diameters, and as all five orifices face a similar overall spray direction, different eccentrical arrangements. The completely asymmetrical nozzles are hardly comparable with literature as the research is focused on automotive and heavy-duty engines. Fig. 1 shows a schematic of a typical fuel injector and its mounted nozzle tip (i) together with a 4:1 enlarged detail on the five orifices in the nozzle tip (ii). Experiments and CFD simulations have shown that the sprays of these asymmetrical nozzles are deflecting significantly and hence, complicate the nozzle design to prevent high

* Corresponding author at: Chalmers University of Technology, Department of Mechanics and Maritime Sciences, Göteborg, Sweden.
E-mail address: balz@chalmers.se (R. Balz).

https://doi.org/10.1016/j.fuel.2021.120455
Received 21 September 2020; Received in revised form 9 January 2021; Accepted 5 February 2021
Available online 8 March 2021

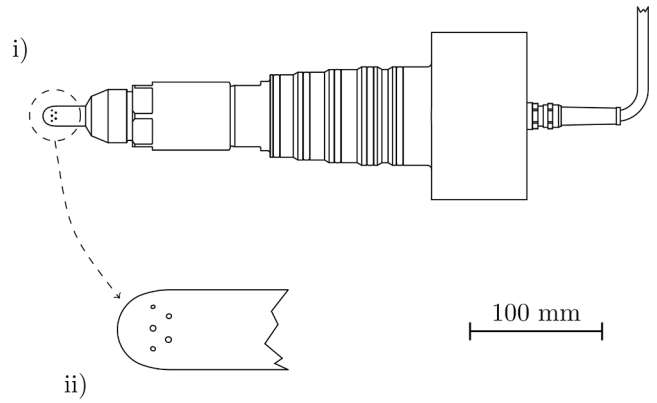

Fig. 1. Schematic top view illustration of a standard fuel injector with mounted nozzle tip (i) as used in large marine two-stroke Diesel engines and enlarged (4:1) detail of the nozzle tip with its five orifices with diameters of 0.75, 0.8, 0.825, 0.85, and 0.75 mm (top to bottom) (ii).

component temperatures [3–6]. These unwanted spray deflections occur mainly due to in-nozzle cavitation flow leading to inhomogeneous velocity distributions at the orifice exits. Introducing radii between nozzle main bore and orifices significantly reduces the amount of cavitation due to enhanced flow resistance, however, certain inhomogeneities of the flow profiles at the exit of the orifices remain.

The influence of this inlet radii on the spray formation and consequent combustion under real engine conditions is of great importance to further deepen the understanding of the nozzle design and hence, improve the fuel injection process to optimize engine efficiency and reduce emissions.

To examine the influence of the in-nozzle flow on the spray morphology and combustion a set of sharp-edged and hydro-erosive ground single-orifice nozzles have been investigated in a constant-volume chamber. The nozzle geometries have been manufactured out of transparent plastic and metal, to get both, the in-nozzle flow information together with the spray and combustion behaviour.

Visualizing in-nozzle cavitating flow in fuel injectors has been a popular research topic over the last decade. Due to the need for refractive index matching of the fuel and transparent material used, only a very limited number of transparent materials are available. Quartz glass and polymethyl methacrylate (PMMA) are the most used materials and the trend in literature aims towards more and more realistic fuel pressures and original-sized nozzle geometries. Especially in the last years, very interesting in-nozzle flow cavitation results were achieved under realistic fuel pressure and nozzle geometry conditions [7–9]. [10,] and [11,] provide an up-to-date review on the experimental non-intrusive investigation of fuel injector phase changing flow. However, the research focus remains on small- and medium-sized engine fuel injection systems, which significantly differ from large two-stroke marine Diesel engines. An exception is the work from [12] and [13], but the experimental in-nozzle flow data remains at very low pressures and/or scaled nozzle geometries were used.

Characterising spray morphology, combustion behaviour and flame propagation of fuel injector nozzles is an established experimental approach for decades [14–18]. Due to the still existing difficulties with predictive CFD spray simulations of the fuel injection process, the importance of experimental spray and combustion investigations in spray chambers remains inevitable. The available data for large two-stroke marine Diesel conditions remains fairly limited since the research on spray and combustion is focused rather on heavy-duty and small-sized engines. Current spray and combustion investigations on larger constant-volume chambers that mimic marine Diesel engine geometries are available, but rather focused on medium bore, four-stroke marine Diesel engines with bore diameters smaller than 300 mm and without swirl motion of the charged air [19–21]. An alternative to spray chambers are on-engine investigations using optical access into the combustion chamber. [22] present interesting flame propagation results on a large two-stroke marine Diesel engine using this approach. However, the limited size of existing spray chambers and the costly operation and limited optical access into the combustion chamber of test engines led Winterthur Gas & Diesel Ltd. (WinGD) to develop and build a constant-volume spray chamber to fit the geometries of large two-stroke marine Diesel engines and their comparatively very large fuel spray and flame structures. The so-called spray and combustion chamber (SCC) is located in Switzerland [23,24] and was used to investigate, among others, the spray morphology and combustion characteristics of different nozzle configurations, fuel types and gas conditions. One of the specialities of the SCC compared with other constant-volume chambers is the possibility to create swirl motion of the charged air which is a highly significant aspect in large two-stroke marine Diesel engines.

Three single-orifice nozzle types have been selected based on the design characteristics of the five-orifice nozzles from large two-stroke marine Diesel engine fuel injectors. This simplification has been chosen to reduce the complexity of the problem by eliminating orifice-to-orifice flow interactions, decrease the failure probability of the plastic transparent nozzles, enhance image quality by preventing orifice intersections on the optical axis, and reduce computational costs of CFD calculations for validation purposes. The three simplified single-orifice nozzle designs have an identical orifice diameter of 0.75 mm and the orifices are arranged centrically and orthogonally (N101), eccentrically and orthogonally (N104), and centrically and angled (N105). These three nozzles have been hydro-erosive ground to create a smooth transition between the nozzle main bore and the orifice by creating inlet-radii and hence, a total of six nozzles have been investigated in this study. The nozzle geometries are described in more detail in Chapter 2.2. The in-nozzle flow has been visualized using transparent nozzles made from polymethyl methacrylate (PMMA) and a transparent nozzle holder that applies uniformly distributed forces to decrease the failure probability of the plastic nozzles (design based on [25]). The experimental and optical setup used to acquire the averaged in-nozzle flow images depicted in Fig. 2 are described in [9]. The experimental conditions were kept strictly identical with exception of the temperature that remained ambient due to decreased material strength of the already critical PMMA. However, experiments have shown that the fuel temperature is qualitatively insignificant for the strong cavitation patterns of the sharp-edged nozzles [26]. The six images in Fig. 2 show the sharp-edged (no HG) and hydro-erosive ground (HG) orifice of the three nozzle types N101, N104 and N105 (see Chapter 2.2 for more information). The selected image section is illustrated as FOV_{IF} in Fig. 3, note the 90° clockwise rotation for visibility reasons. The shown images are averaged over the quasi-steady-state fuel injection and therefore, the cavitation pattern seems blurry. The back-illuminated images show gaseous flow, i.e. cavitation, as dark areas within the walls of the orifice. The bright areas within those walls represent liquid flow as the light is not refracted off the optical axis due to refractive indices differences. Note that the orifice walls are visible as dark lines as well since the Diesel fuel used has only a very similar, but not perfect identical refractive index as the PMMA of the transparent nozzles. The fuel enters the nozzle main bore from the top left side, enters the orifice, and flows downwards towards the exit of the orifice at the bottom of the images.

The level of hydro-erosive grinding can be determined by the enlarged orifice diameters and non-symmetric orifice inlet radii. These geometrical properties decrease the level of cavitation significantly. The three nozzle types with the sharp-edged orifices all show super-cavitation: the geometrical cavitation is reaching the exit of the orifice [11]. After hydro-erosive grinding of the three nozzle types, only the eccentric nozzle N104 indicates that cavitation reaches the exit of the orifice during the quasi-steady-state fuel injection. The other two nozzle types show cavitation only around the orifice inlet: nozzle N101 on both inlet sides and only around a quarter of the orifice length and nozzle N105 only on one side and around half of the orifice length.

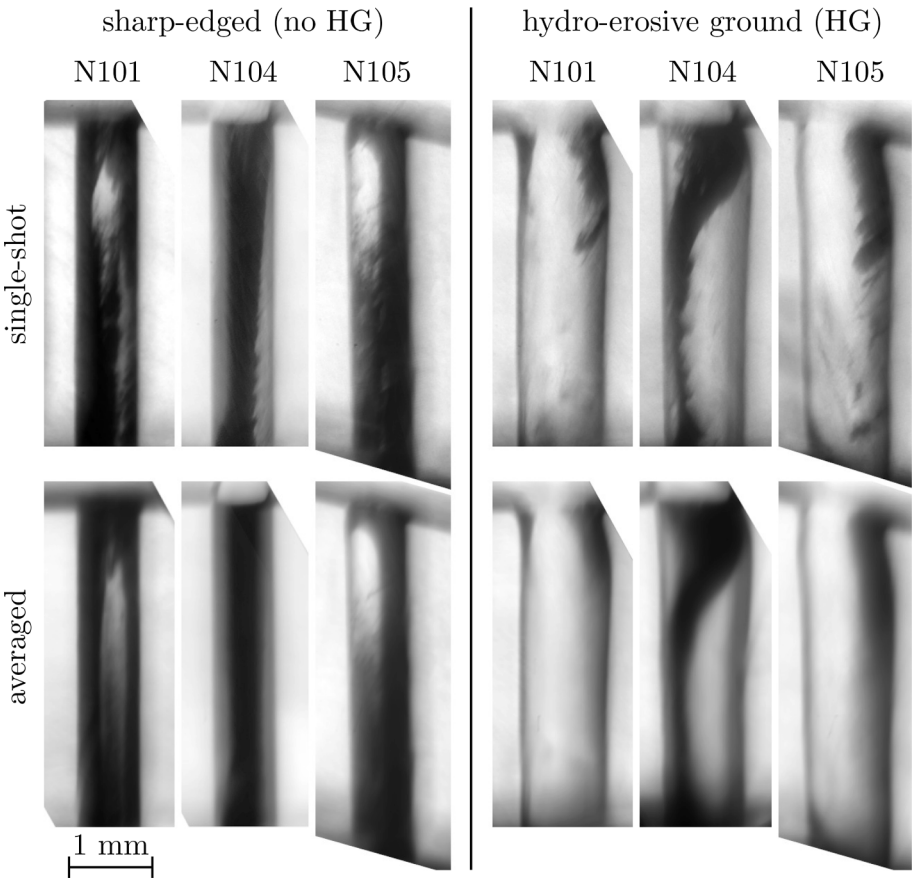

Fig. 2. Experimental in-nozzle flow images of the six nozzles investigated acquired with identical fuel and rail pressure of 50 MPa. The images are averaged over the quasi-steady-state fuel injection period. Dark areas within the borders of the orifice and main bore represent gaseous flow, e.g. cavitation while bright areas within the orifice borders represent liquid flow. The angled nozzle type N105 has been rotated for visualization purposes. The fuel enters the main bore from the left side, flows vertically through the orifice and leaves the orifice at the bottom of the image. Data partly from [9].

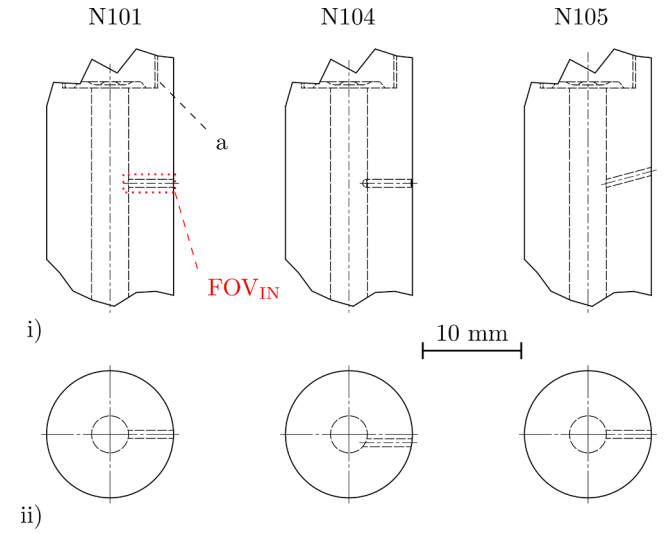

Fig. 3. Schematic illustrations of the three different nozzle types used with detailed side view (i) and top view (ii). Note that the shown drawings represent the sharp-edge design, i.e. non-hydro-erosive ground nozzles. The mounted pressure transducer is depicted at the end of the main bore on top of the nozzles (a). The red dotted FOV_{IN} illustrates the selected field of view for the in-nozzle flow images (see Chapter 1).

Additionally, the hydro-erosive ground (HG) nozzle N104 shows a very significant cavitation swirl pattern that remains unique among the nozzles investigated. The in-nozzle flow experiments and data are described in more detail in [9].

2. Experimental setup

2.1. Spray and combustion chamber (SCC)

The experiments were performed in the state-of-the-art constant-volume spray and combustion chamber (SCC) at WinGD. The inner geometry represents the combustion chamber at top dead center of a RT-flex50 engine with an bore size of 500 mm. Optical access is provided by multiple sapphire windows with a maximum visible diameter of 150 mm. Using a regenerator consisting of multiple heating plates and heat exchanging area, and two high-pressure air bottles at around 30 MPa, the opening time of two solenoid driven, fast valves define the pressure and temperature of the air in the spray chamber. This filling process to create the combustion atmosphere also allows to create the strong swirl motion of the charge that is necessary to have identical operating conditions before fuel injection as exist on the engines. After each injection, the charge is released through an exhaust valve and the pressure bottles are filled up again, using an air compressor, to restart the process. The SCC is described in more detail in [23,24].

For the experiments presented in this study, the SCC operating conditions were set to 9 MPa back pressure (before injection) at a temperature of 900 K and a swirl velocity of approximately 20 m/s. The SCC cover was heated to approximately 450 K to simulate the cylinder wall temperatures. The pressure and temperature in the SCC are measured using piezo-capacitive pressure transducers (Kistler 7061BS31) and fast type K thermocouples. The pressure and temperature conditions would be in the range of a 50% engine load point with R1 rating of a RT-flex50 engine (bore of 500 mm, stroke of 2050 mm, rotating speed between 99 to 124 rpm, mean effective pressure of 2 MPa at R1 rating, and piston speed of 8.5 m/s). The injection duration is of a lower load point in order to reduce the amount of injected fuel during the experiments. From the point where the spray is quasi-steady-state,

the information on the interaction between the in-nozzle flow and spray/combustion is seen to be stable and a prolonged injection will not yield to additional insights.

A standard Swedish Diesel fuel (Preem AB, DMK1UA-SE) with a density of 815.9 kg/m^3 (at 15 °C), a kinematic viscosity of 2.112 mm^2/s (at 40 °C) and a net heat of combustion of 43.16 MJ/kg was used using a media separator (high pressure piston accumulator) and a standard high pressure pump, rail, and injection control unit (ICU), as used on the engines of WinGD. The rail pressure was set to 50 MPa and the injector used was a WinGD standard solenoid injector manufactured by L'Orange. The injection duration was set to 12 ms.

Fifteen fuel injections have been recorded per nozzle type, resulting in a total of 90 experimental cases. The SCC conditions were kept constant for each injection. The fifteen fuel injections per nozzle have been used to average the evaluated data and calculate the standard deviation.

2.2. Nozzle geometries

The nozzles used are single-orifice nozzles based on the five-orifice nozzle designs used on engines from WinGD. There were three different nozzle types investigated without and with hydro-erosive grinding, resulting in a total of six data sets acquired. The non–hydro-ground nozzles have an identical orifice diameter of 0.75 mm and the orifice orientation represents the basic arrangement on the real, five-orifice nozzles used on WinGD engines. The nozzle N101 has a centrically arranged, orthogonal orifice, nozzle N104 an eccentrically arranged, orthogonal orifice and the nozzle N105 a centrically arranged but angled orifice.

The simplification of using one instead of five-orifice nozzles enables a better assessment since the in-nozzle flow and sprays are not interacting. Additionally, the computational time for CFD validation is significantly reduced and the optical acquisition is massively simplified since the individual sprays would block each other with the applied line-of-sight optical measurement technique and as a result limit valuable information. This simplification approach complicates the approach of extending the experimental results to real nozzle designs, as the level of turbulence within the fuel injector and nozzle is reduced by the lower mass flow and hence fuel velocities. Additionally, no flow interactions between the orifices can occur that also can influence the cavitation behaviour. However, the gained information is valuable, as the in-nozzle flow investigations have shown that the steady-state cavitation patterns are quite steady and insensitive to pressure fluctuations [9], and the main interest of this study is the influence of the cavitating in-nozzle flow on the spray and combustion behaviour.

To guarantee similarity regarding pressure conditions in the nozzle tips, the in-nozzle pressure has been measured using a piezo-resistive transducer (Kistler 4067E) mounted on top of the nozzle main bore at ambient conditions. For the combustion experiments, the sensor has been replaced with a dummy. The location of the sensor is depicted in the schematic illustration of the three different nozzle types used in Fig. 3.

The exact geometrical details of the three different, non–HG nozzle geometries are presented in Table 1 together with the hydro-erosive grinding specifications applied. Using hydro-erosive grinding (HG) to create the inlet radii between main bore and orifice, the three nozzle types N101, N104, and N105 were HG and characterised by evaluating their mass flow properties using a calibration oil (Castrol Calibration Oil 4113) at a pressure of 5 MPa on a flow rig. The metal nozzles were HG until the flow properties matched the values of the transparent nozzles used for the in-nozzle flow visualizations as described in chapter 1.

Table 1
Geometrical properties of the sharp-edged and hydro-erosive ground (HG) nozzles used.

		N101	N104	N105
main bore diameter	[mm]	3.5	3.5	3.5[t]
orifice diameter	[mm]	0.75	0.75	0.75
orifice eccentricity	[mm]	0	0.8	0
orifice angle	[deg]	90	90	75
mass flow at 5 MPa	[g/s]	18.9	28.9	21.0
orifice exit diameter after HG	[mm]	0.98	0.92	0.95
mass flow at 5 MPa after HG	[g/s]	31.0	41.1	33.0
extruded HG fluid	[g]	150.5	194.8	203.4

A commercially available working fluid from Gradnings & Maskinteknik AB (EM-70760-W/120S) has been used to hydro-erosive grind the nozzles made from stainless steel (1.4301). The hydro-erosive grinding fluid achieves highly repeatable results due to a homogeneous mixture of the fluid and abrasive particles and the relatively long grinding times at low differential pressure. The fluid/abrasive particle mixture has been pushed through the nozzles with a static differential pressure of 1.5 MPa to match a defined mass flow measured at 5 MPa, as provided in Table 1.

The excessive level of hydro-erosive grinding produces a complex, flow optimized geometry which consists of multiple interconnected radii that lead to tapered and slightly oval shaped orifices. The complex three dimensional shape of the HG in-nozzle geometries can currently not be quantified. However, to reproduce the nozzle geometries, the averaged used mass of the hydro-erosive grinding fluid (collected at the nozzle orifice exits), the exit orifice diameters, and the mass flow evaluated at 5 MPa are provided in Table 1.

2.3. Optical setup

An optical light probe (OLP) prototype from Kistler with a 305–315 nm bandpass filter and a photomultiplier was used to evaluate the start of ignition (SOI) with a high temporal resolution of 1 MHz. Two high-speed CMOS cameras (Photron HSS6) were used in an alternating setup together with a lens-coupled image intensifier (LaVision IRO) and a diode laser as a light source (Cavitar Cavilux Smart). Using an alternating setup with the two available high-speed cameras, the four following datasets using different field of views (FOV) and acquisition rates were acquired:

1. diffuse back illumination (20 kHz, optical setup I, FOV_I)
2. flame luminescence (20 kHz, optical setup I, FOV_I)
3. diffuse back illumination (100 kHz, optical setup II, FOV_{II})
4. OH*-chemiluminescence (40 kHz, optical setup II, FOV_{III})

The different acquisition rates vary in different FOV and thus, the optical setup II is zoomed in towards the exit of the nozzle orifice while the optical setup I shows the maximal FOV provided by the optical window. The schematics of the optical setups are depicted together with the SCC as top view in Fig. 4 and side view in Fig. 5. The top view in Fig. 4 shows the SCC (b) with part of the regenerator (g) and the mounted injector (a). The optical setup around the SCC consists of the light source on one side; diode laser (f), light fibre (e), and collimator (d) together with a diffuser plate (c). On the other side are the high-speed cameras (h, n, q) with their individual mirrors (s, t, u), lenses (r, o, l), and filters (p, m). Note that all three cameras are depicted, although an alternating optical setup has been used. The optical setup I used the camera (q) and camera (n) while the optical setup II used the camera (h) and camera (n); the camera (q) and (h) were switched and the collimator (d) adjusted for the two different optical setups.

To acquire the line-of-sight diffuse back illumination images, the camera (n) together with a Nikon zoom lens (o) and a 690±10 nm bandpass filter (p) have been used together with the diode laser (f). The OH*-chemiluminescence used a Cerco UV-lens (l) with a mounted 305–315 nm bandpass filter (m) in front of the image intensifier (k). The flame luminosity has been acquired using a Nikon zoom lens (r) with closed aperture. Using differently coated mirrors allowed the use of one single optical axis; mirror (u) reflects below 370 nm, the mirror (t) reflects below 700 nm and mirror (s) is a broadband mirror.

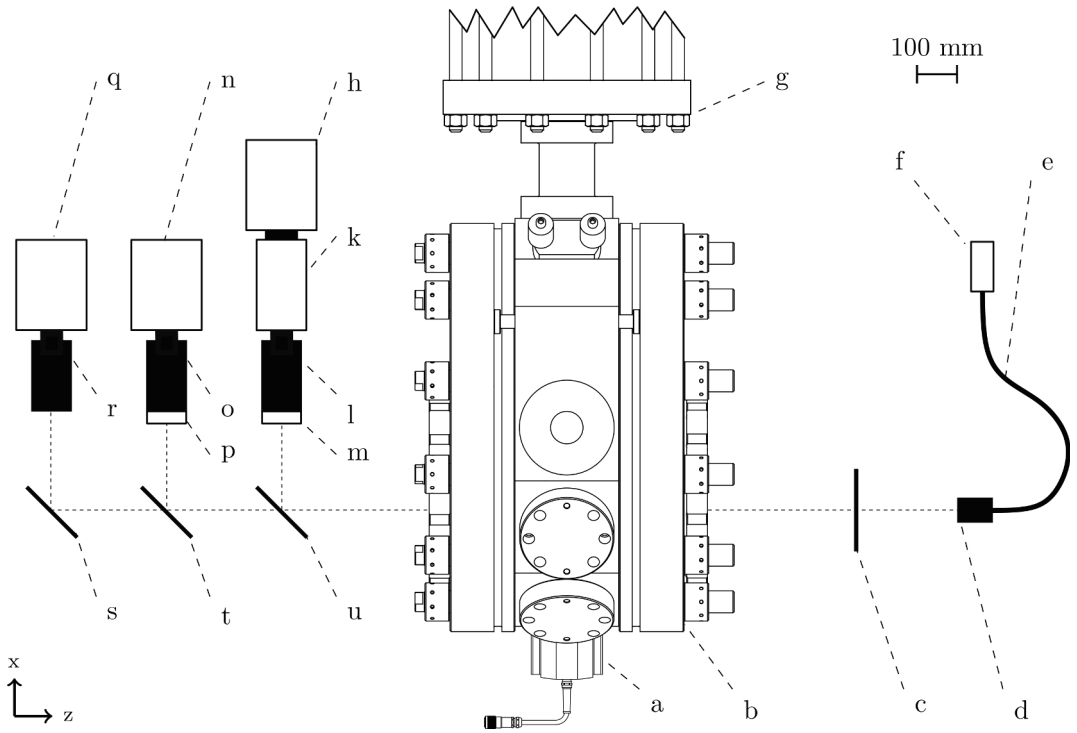

Fig. 4. Schematic top view of the spray and combustion chamber (SCC) with the optical setup. Fuel injector (a), SCC main body (b), diffuser plate (c), collimator (d), light fibre (e), diode laser (f), SCC regenerator (g), high-speed camera 1 (h) with image intensifier (k), UV lens (l) and filter (m), high-speed camera 2 (n) with lens (o) and filter (p), high-speed camera 3 (q) with lens (r), mirror (s), mirror (t) and high-pass filter (u).

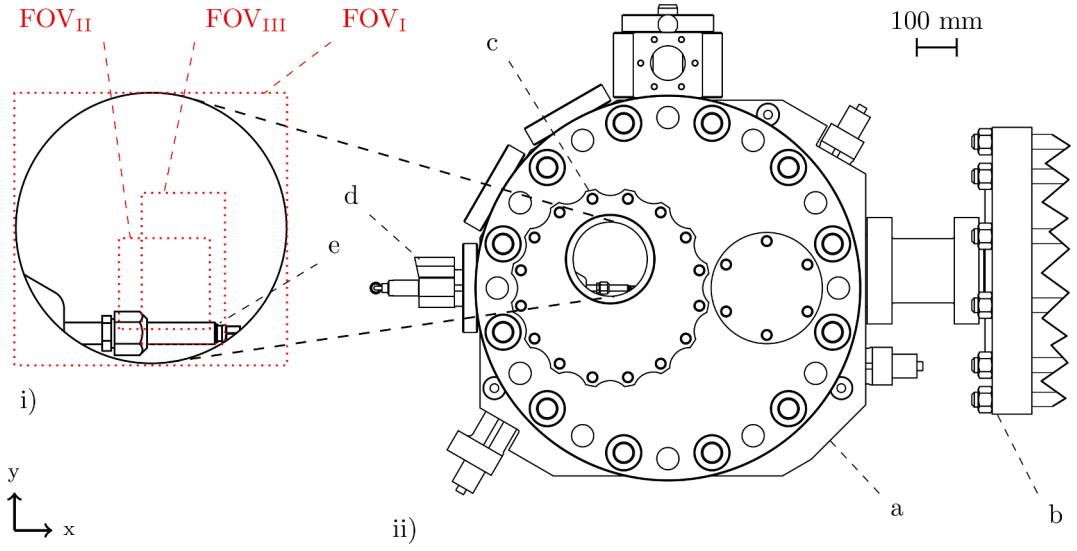

Fig. 5. Schematic side view of the spray and combustion chamber (SCC) (ii) indicating the optical access and the enlarged view through the optical windows with the three different field of views (FOV) used (i). SCC main body (a), SCC regenerator (b), side flange with optical access through sapphire windows (c), fuel injector (d), and nozzle (e). The three different fields of view (FOV$_{I}$, FOV$_{II}$ & FOV$_{III}$) are illustrated using dotted rectangles in the detailed view (i).

The three different FOV are depicted together with a schematic side view of the SCC in Fig. 5. The SCC (a) with the mounted injector (d) and window holder (c) as well as the regenerator (b) are illustrated in ii) while the optical access showing the nozzle tip (e) together with the three different FOV$_{I-III}$ is enlarged in i). The main advantage of using the alternating setup is the available 100 kHz diffuse back illumination data which reveals more temporal information. This is especially interesting for spray penetration and the hydraulic start of injection evaluations. On the other hand, the maximal FOV is also interesting to analyse the flame and spray contours. As the high-speed camera hardware required reduction of the FOV to achieve the high acquisition rate leads to an information loss usually only limited by the optical access of the SCC, the alternating optical setup has been chosen to get both, high temporal and high spatial resolution.

2.4. Image analysis

The acquired images have been evaluated using Matlab based on the standard routines as described in more detail in various work [14,15,27,20]. Fig. 6 shows the evaluation sequence of a typical spray

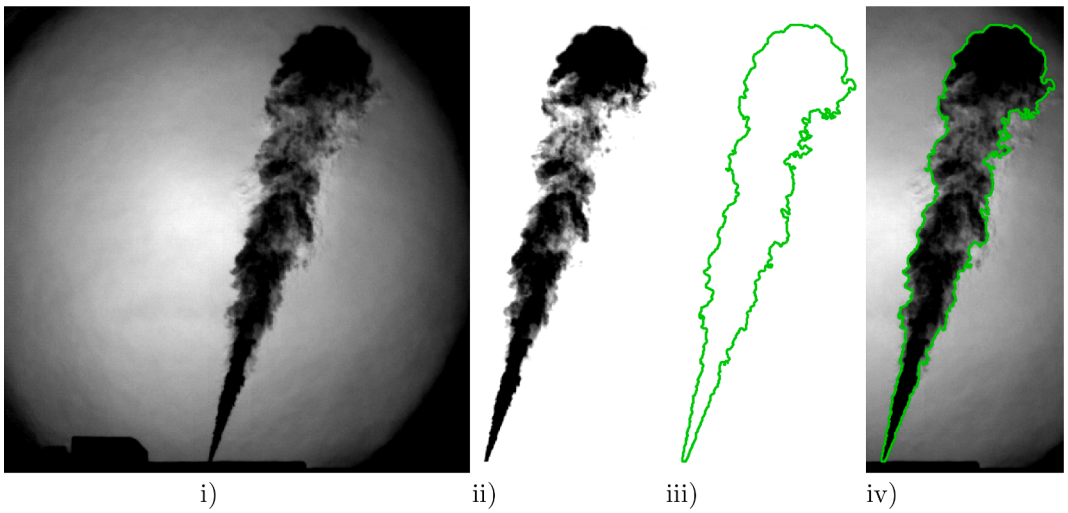

Fig. 6. Image evaluation showing the raw diffuse back illumination image of FOV_I during fuel injection i), background adjusted and cropped image ii), evaluated contour iii) and contour overlaid with cropped raw image iv).

image. Image i) shows a raw image during injection with an ignited spray. The image is a diffuse back illumination from the optical setup I with FOV_I. The spray/flame is isolated by background homogenisation and mapping as well as cropping (ii). Using a threshold, the spray/flame contour is then evaluated using the Moore-Neighbor tracing algorithm modified by Jacob's stopping criteria [28]. Image iv) shows the evaluated contour with the cropped, raw image to demonstrate the accuracy of the method for the acquired images.

The diffuse back illumination images alone impede the evaluation of the flame location, especially during the transient fuel injection at start of ignition and close to the flame-lift-off length, where the spray remains still very dense. Therefore, the flame luminosity images have been evaluated using the same method to use the flame contour to analyze the geometrical flame properties. The evaluated contour data of the spray and the flame allows to analyze the data regarding their spray morphology like spray penetration, spray angle, flame-lift-off length, spray and flame contour, flame area, etc.

3. Results & discussion

3.1. General

The influence of the hydro-erosive grinding (HG) and thereby reduced flow resistance can be visualized by plotting the in-nozzle pressure curves during the fuel injection. Fig. 7 shows the normalized (rail pressure of 50 MPa) six in-nozzle pressure curves measured under ambient back-pressure and temperature conditions together with the solenoid current of the fuel injector. The solid lines represent the non-–hydro-erosive ground, i.e. sharp-edged (no HG) and the dashed lines show the pressure curve for the HG nozzles. The data is averaged over multiple injections and is very stable and reproducible. The pressure fluctuations during the quasi-steady-state fuel injection between approximately 6 to 14 ms originate from the fuel system (rail, valves, pipes, and injector) and are accurately reproducible as well. For visibility reasons, the standard deviation which has not been plotted in Fig. 7. However, a value during the quasi-steady-state fuel injection process is provided in Table 2. The plot impactfully shows how the pressure rise extenuates with HG, especially for the eccentric nozzle N104. This effect occurs due to the reduced flow resistance by creating smooth inlet radii using HG. The change in flow resistance also leads to changes in the averaged pressure during the quasi-steady-state injection period, and in the pressure decrease during needle closing. For both versions of the nozzles, the sharp-edged and the HG, the eccentric nozzle N104 stands out: the in-nozzle pressure development remains very

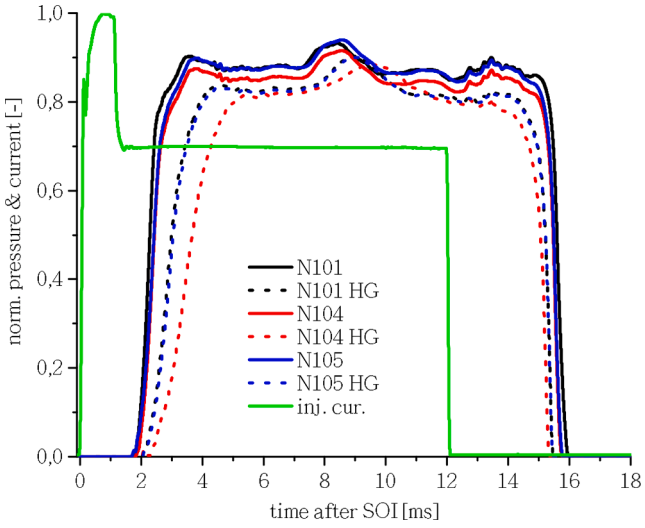

Fig. 7. Normalized and averaged injection current and in-nozzle pressure for the three sharp-edged (no HG) and hydro-erosive ground (HG) nozzle types measured.

similar for the standard and angled nozzle N101 and N105, while the eccentric N104 has a lower pressure when sharp-edged, and an even further reduced pressure rise time when HG.

The injected mass of the nozzle types has been simultaneously measured with the in-nozzle pressure. Using a metal pipe to dissipate the spray energy and collect the fuel, the injected mass has been gravimetrically evaluated over 100 injections for each nozzle type with and without HG. The data shows that the standard, sharp-edged nozzle N101 has the lowest and the eccentric, HG nozzle N104 by far the highest mass flow. The injected mass between HG, angled nozzle N104, and HG, standard nozzle N101 is almost identical, which also reflects with the matching curves in the in-nozzle pressure plot depicted in Fig. 7. Note that the injected mass values are slightly increased, as measured under ambient temperature and back-pressure conditions.

The averaged in-nozzle pressures during the quasi-steady-state fuel injection of the various nozzle types and the evaluated injected masses are shown in Table 2.

Table 2
Measured characteristics for the three sharp-edged and the three hydro-erosive ground nozzles. The data shown are the mean (μ) values together with the standard deviation (σ) evaluated during the quasi-steady-state fuel injection period over multiple injections.

		sharp-edged (no HG)						hydro-erosive ground (HG)					
		N101		N104		N105		N101 HG		N104 HG		N105 HG	
		μ	σ	μ	σ	μ	σ	μ	σ	μ	σ	μ	σ
in-nozzle pressure	[bar]	378.9	8.2	368.9	9.4	379.0	9.5	360.5	14.3	357.3	14.7	359.4	14.5
injected mass	[g]	0.667	0.013	0.892	0.017	0.874	0.019	1.425	0.032	1.914	0.012	1.411	0.052
flame lift-off length	[mm]	24.8	4.4	31.5	5.0	30.9	4.6	38.4	6.9	29.1	3.5	37.6	5.2
start of ignition	[ms]	0.30	0.01	0.47	0.03	0.39	0.04	1.06	0.06	1.24	0.1	1.05	0.13
spray angle	[deg]	14.5	0.8	16.4	2.1	14.2	0.9	16.3	0.4	23.3	0.8	17.2	1.1
spray axis	[deg]	+ 0.9	0.2	−0.7	0.5	−0.9	0.2	+ 0.4	0.3	+ 1.2	0.3	+ 0.6	0.3

3.2. Spray morphology

Using the spray analysis presented in Chapter 2.4, the evaluated spray contours acquired using diffuse back illumination with 100 kHz within the FOV_{II} have been used to investigate typical spray morphology quantities.

The different spray contours have been averaged and plotted individually for the three nozzle types used and are depicted in Fig. 8. The spray contours have been averaged over the quasi-steady-state fuel injection period, as described in the previous chapter, and over multiple fuel injections. The contour data is cropped in y-direction at approximately 25 mm which represents the shortest flame lift-off length of all six nozzle types investigated. This guarantees that the evaluated spray contours represent only the fuel spray and are not affected by the flame contours.

The spray angle is proportional to the nozzle diameter and widens with increasing values [29]. As the hydro-erosive grinding process enlarges the orifice diameters significantly, all three nozzle types show widened spray angles with HG, as the red curves indicate in Fig. 8. While the expanded spray contours remain fairly symmetrical for the standard and angled nozzle types N101 and N105, the eccentric layout significantly alters the contour asymmetrically.

The averaged spray angles have been evaluated at a distance from the orifice exit of 15 times the orifice diameter and are provided together with the evaluated spray axis in Table 2.

The eccentric nozzle N104 has by far the widest angle while the standard nozzle N101 generates the narrowest. The widening up of the sprays with HG can be explained with the increased orifice diameters induced by the HG [30,31] (compare with in-nozzle flow images in Fig. 2). However, for the eccentric case, the increasing level of cavitation swirl motion within the orifice dominates the influence on the spray formation. This special in-nozzle flow cavitation pattern can be seen in the in-nozzle flow visualizations as depicted in Fig. 2. The in-nozzle swirl effect on the spray can be seen in the atypical spray contour in Fig. 8 (middle), where the spray significantly inflates close to the orifice exit on the positive x-axis. The rather symmetrical spray contour of the sharp-edged, eccentric nozzle indicates that the in-nozzle swirl motion intensifies with HG which can also be seen in the in-nozzle flow images depicted in Fig. 2 where the non–HG N104 nozzle shows no swirl behaviour but very extended level of supercavitation [32].

Comparing the in-nozzle flow images of the nozzle N101 and N105 as depicted in Fig. 2 with the corresponding spray contours as presented in Fig. 8 results in differences that are not as distinctive as with nozzle N104. For nozzle N101 which is supercavitating before HG and only shows very small geometrical cavitation after HG, the spray angles widens up quite symmetrically. For the angled nozzle N105 which shows very dominant cavitation behaviour on one side of the orifice only, the spray angle widens up as well, but not as distinctive as with the other two nozzle types (see Fig. 8). However, the nozzle N105 changes the spray axis significantly with HG and leads to a reduced nominal angle of the nozzle design.

3.3. Combustion

Fig. 9 shows typical, unedited, flame luminosity and diffuse back illumination images of the sharp-edged and the hydro-erosive ground

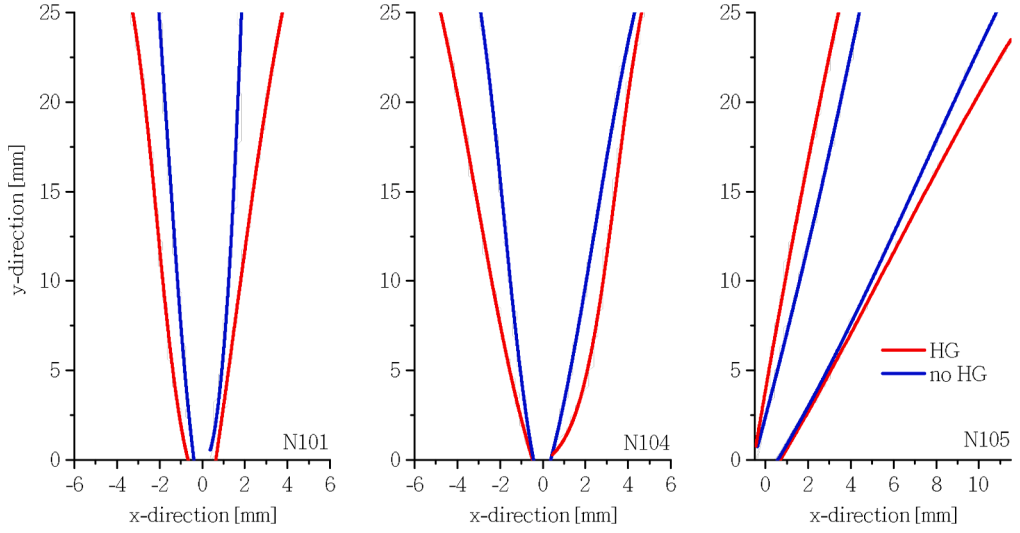

Fig. 8. Spray contours comparison between sharp-edged (no HG) and hydro-erosive ground (HG) nozzles of the standard type N101 (left), the eccentric type N104 (middle), and angled type N105 (right). The contours have been averaged over the quasi-steady-state fuel injection from data of multiple injections. Note that the scaling of the axes is arbitrary, and the raw data (black line) has been curve fitted.

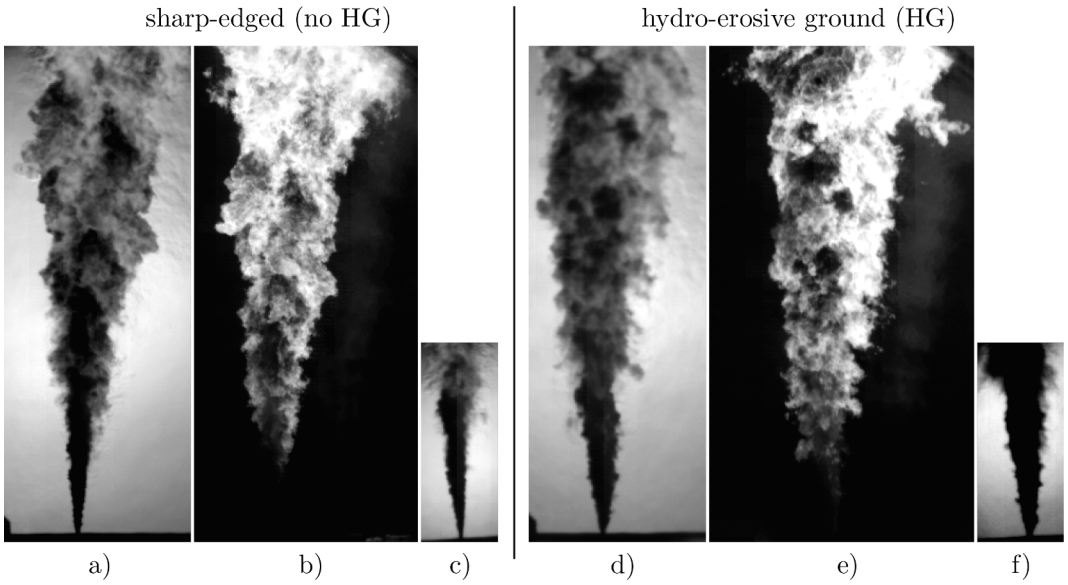

Fig. 9. Typical acquired flame luminosity and diffuse back illumination images for sharp-edged (no HG), and hydro-erosive ground (HG) version of the nozzle N104. a) and d) shown the diffuse back illuminated spray acquired with 20 kHz in FOV_I, b) and e) show the flame luminosity in FOV_I, and c) and f) show the diffuse back illuminated spray acquired with 100 kHz in the reduced FOV_{II}.

nozzle N104 during the quasi-steady-state fuel injection. The wider spray angle with the hydro-erosive ground nozzle, as described in the previous chapter, can be distinguished by comparing the diffuse back illumination images acquired with 20 kHz in a) and d), and also by comparing the diffuse back illumination images acquired with 100 kHz in the reduced FOV_{II} in c) and f).

Fig. 9 b) and e) show typical flame luminosity images acquired with 20 kHz during the quasi-steady-state fuel injection. Note the slightly larger flame area and shorter flame lift-off length with the hydro-erosive ground nozzle in Fig. 9 e). The two images match the exact timing of the diffuse back illumination images a) and d), and although the FOV is slightly different, a comparison reveals identical flame contours. Using both optical measurement techniques helps to distinguish the differences between flame and spray.

By using the image analysis technique presented in Chapter 2.4 on the images acquired using the flame luminosity optical setup, the flame lift-off length during the quasi-steady-state fuel injection has been evaluated. The start of ignition (SOI) has been measured using the OLP, as it had higher temporal resolution than the OH*-chemiluminescence optical setup which has been used to evaluate the location of the ignition. The averaged flame lift-off length and SOI of the various nozzle types investigated are shown in Table 2. The flame lift-off length has been evaluated as described in [33]. For better visibility reasons, some of the key results shown in Table 2 are also depicted as horizontal bar plots in Fig. 10. The Figure shows the start of ignition (SOI), flame lift-off length, spray angle and the injected mass for the three nozzle types with and without HG.

The start of ignition (SOI) massively delays with HG no matter the nozzle type. The sharp-edged, standard nozzle N101 has the most repeatable and earliest SOI while the HG, eccentric nozzle N104 has the latest. HG roughly triples the SOI time, which can be explained with the reduced level of atomization due to improved flow resistance and due to the enlarged orifice diameter resulting in roughly double the injected fuel mass. It is reported that larger orifice diameters lead to slightly shifted size-volume distributions of the atomized droplets. The curves move towards larger fuel droplet diameters with increasing orifice diameter and hence reduce the level of spray atomization [34].

Regarding injected mass, the sharp-edged, standard nozzle N101 has the lowest amount per injection where the other two sharp-edged nozzle types have a very similar value. The difference in mass flow is approximate −25%, which is substantial given that all three sharp-edged nozzle types have an identical orifice diameter of 0.75 mm. Although the nozzles were equally long hydro-erosive ground, the mass flow changes irregular; the eccentric nozzle N104 achieves by far the highest and most

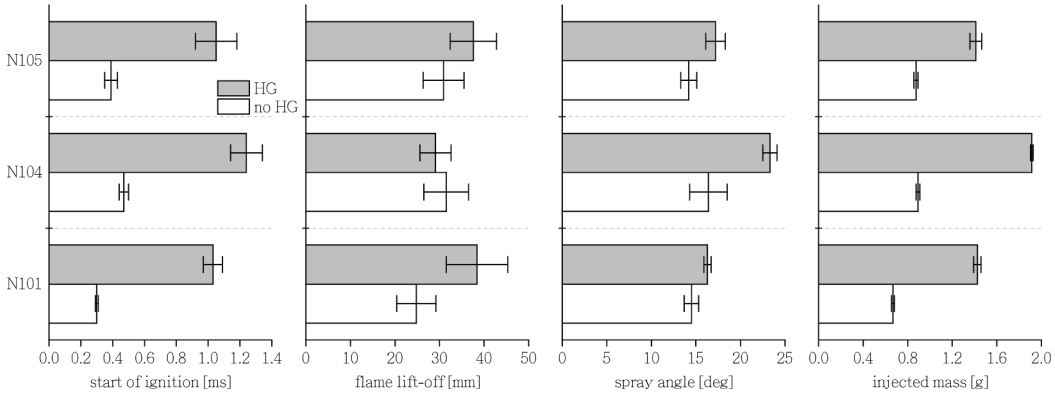

Fig. 10. Start of ignition, flame lift-off, spray angle and injected mass for the three different nozzles N101, N104 and N105, sharp-edged (no HG) and hydro-erosive ground [HG].

repeatable, viz. stable mass flow (lowest standard deviation). This can be explained with the characteristic in-nozzle cavitation swirl motion as shown in Fig. 2, which leads to a beneficial and more stable velocity pattern with regard to an increased and low fluctuating discharge behaviour.

The flame lift-off length of the sharp-edged, standard nozzle N101 is the shortest, matching the findings for SOI and injected mass. This behaviour is linked and can be explained with the enhanced level of atomization due to the sharp-edge nozzle design. The resulting increased level of atomization accelerates fuel evaporation and hence, affects the ignition and combustion behaviour. Decreased turbulence due to increased nozzle diameter and flow optimization due to HG lead to a reduced level of spray atomization [35–37]. This effect together with the massively reduced in-nozzle cavitation level as depicted in Fig. 2 weaken the spray breakup and result in prolonged flame lift-off lengths with HG. It is also reported that increasing orifice diameters lead to an increased flame lift-off length [30]. However, the flame lift-off length changes anomalous with HG for the three different nozzles. While it elongates with HG for the standard (N101) and angled (N105) nozzle types, it slightly shortens for the eccentric nozzle N104. This diverse behaviour fortifies the special relevance of the eccentrically arranged orifice design, which significantly stands out among the three nozzle types investigated, especially in regard to the characteristic in-nozzle flow cavitation pattern. The velocity pattern at the exit of the orifice seems to be significantly enhancing the mixture formation at a more upstream position in the spray.

The ignition location evaluated from the OH*-chemiluminescence data is depicted in Fig. 11 as red marks with standard deviations in x and y direction, together with the averaged spray images, closest to the measured SOI using the OLP signal. Note the indicated, clockwise swirl flow direction within the SCC. The significantly earlier SOI for the sharp-edged nozzles is clearly visible with the smaller and shorter sprays, compared to the much larger and hence, further penetrated sprays of the HG nozzles. The HG version of the eccentric nozzle N104 has the smallest standard deviations indicating a highly repeatable and very firm fuel atomization as well as mixture formation. The swirl motion in the combustion chamber leads to a one-side dominance of the ignition spot for most cases, however, the sharp-edged (no HG) eccentric (N104) and angled (N105) nozzle seem to be the exceptions. The strong swirl flow motion rotates in clockwise direction (compare with schemata of the SCC in Fig. 5) and therefore enhances the spray evaporation towards the negative x-direction (left side in Fig. 11). The denser sprays from the HG nozzles are more prone to this effect, due to the extended SOI of the HG nozzles.

4. Conclusions

The three single-orifice nozzle geometries investigated, representing large two-stroke Diesel engine atomizer design aspects, show extensive differences in spray morphology and combustion behaviour with regard to the effect of hydro-erosive grinding (HG). All three ground nozzle types have enlarged spray angles and higher mass flow rates due to the influence on in-nozzle flow pattern as well as the increased orifice diameters. While literature links the prolonged spray penetration, spreading and enlarged angle to an increasing orifice diameter [38], this work shows that the in-nozzle flow cavitation patterns have a significant influence as well, especially for the eccentric nozzle design with its strong swirl cavitation in-nozzle flow.

The start of ignition is delayed by up to a factor three when HG has been performed. [39] and others also report that an increased orifice diameter delays the start of ignition. However, the in-nozzle flow data available and the spray contour data show that the slight increase of the orifice diameter, due to significant levels of HG, is just one reason for the measured variations in spray morphology and combustion characteristics. This study explicitly describes the effects of in-nozzle cavitation as a very dominant cause as well. Linking the qualitative in-nozzle cavitation flow images with the quantitative spray morphology and combustion results enables a detailed analysis of the fuel injection behaviour, especially for the eccentric nozzle type (N104) with its unique strong swirl cavitation pattern and thus, discharge velocity pattern.

In contrast to the other two nozzle types with HG, the eccentrical nozzle design significantly generates an asymmetrical spray contour while maintaining a similar flame lift-off length when comparing to the non HG case. This in-nozzle cavitation swirl flow driven spray contour leads to a start of ignition location closest to the orifice exit and most reliable in regard its deviation.

The data shows that the HG eccentric nozzle has by far the most injected mass of all three nozzle types given the same level of hydro-erosive grinding. Indicating the high influence of the in-nozzle swirl motion and therefore, a beneficial velocity profile for the discharge. This is also reflected with regard to the spray axis as the eccentric (N104) nozzle reveals the most significant change, while the standard (N101) and angled (N105) nozzle designs have less than half the spray axis deflection after HG.

The detailed in-sight with regard to in-nozzle flow characteristics in relation to the spray morphology as well as subsequent combustion behaviour enables a better understanding of the under-laying phenomena, which is a prerequisite for the further development of the fuel injection as well as combustion system. Furthermore, the data is highly valuable with regard to the validation of numerical spray models and

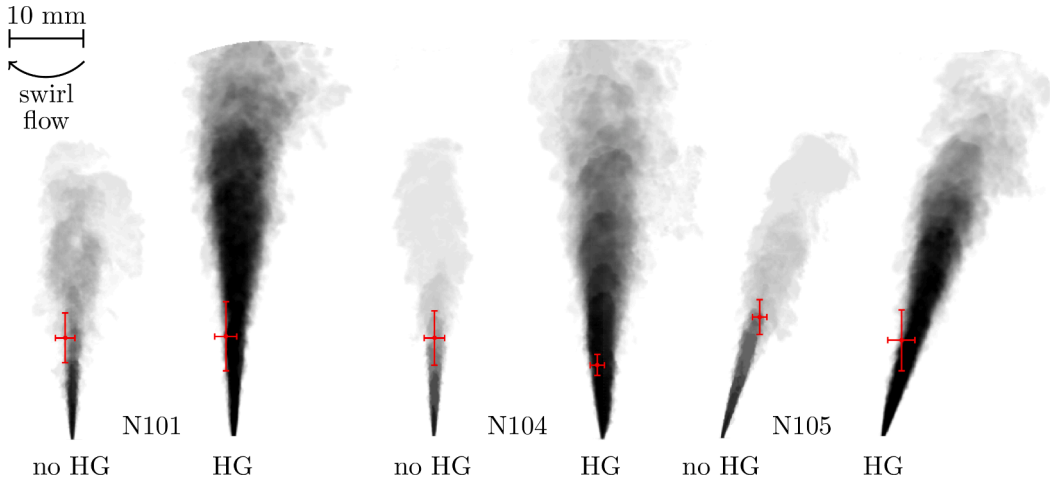

Fig. 11. Averaged spray images with marked location of start of ignition (SOI) for the three nozzle types N101, N104, and N105, both for sharp-edged (no HG) and hydro-erosive ground (HG) versions.

simulation tools, especially, also in the view of upcoming emission regulations as well as the emerging utilization of alternative fuels in such engine types.

CRediT authorship contribution statement

R. Balz: Conceptualization,Writing - original draft. **G. Bernardasci:** Investigation, Data curation. **B. von Rotz:** Writing - review & editing. **D. Sedarsky:** Supervision, Project administration, Funding acquisition.

Declaration of Competing Interest

The authors declare that they have no known competing financial interests or personal relationships that could have appeared to influence the work reported in this paper.

Acknowledgments

The authors would like to thank the Combustion Engine Research Center (CERC) affiliated to Chalmers University of Technology, the Swedish Energy Agency and the Swiss Federal Office of Energy for financial support. Special thanks to Matthias Stark.

References

[1] ETI Energy Technology Institute. Targeting a 30% improvement in fuel efficiency for Marine vessels, Technical Report; 2017.
[2] International Chamber of Shipping. 2017 Annual Review, Technical Report; 2017.
[3] Schmid A, Habchi C, Bohbot J, von Rotz B, Herrmann K, Bombach R, Weisser G. Influence of in-nozzle flow on spray morphology. In: ILASS – Europe, 26th European Conference on Liquid Atomization and Spray Systems, Bremen, Germany; 2014.
[4] Habchi C, Gillet N, Velghe A, Bohbot J, Schmid A, von Rotz B, Herrmann K. On the role of Cavitation in Marine Large Diesel injector: Numerical investigation of nozzle orifices eccentricity. In: ILASS – Europe, 26th Annual Conference on Liquid Atomization and Spray Systems, Bremen, Germany.
[5] Nagy IG, Schmid A, Hensel S, Dahnz C. Computational analysis of spray primary breakup in 2-stroke marine diesel engines with different nozzle layouts. In: ICLASS, 13th Triennial International Conference on Liquid Atomization and Spray Systems, Tainan, Taiwan; 2015.
[6] Nagy IG, Matrisciano A, Lehtiniemi H, Mauss F, Schmid A. Influence of Nozzle Eccentricity on Spray Structures in Marine Diesel Sprays, SAE Technical Paper Series 2017-24-0031; 2017.
[7] Kirsch V, Hermans M, Schönberger J, Ruoff I, Willmann M, Reisgen U, Kneer R, Reddemann M. Transparent high-pressure nozzles for visualization of nozzle internal and external flow phenomena. Rev Sci Instrum 2019;90.
[8] Gomez Santos E, Shi J, Gavaises M, Soteriou C, Winterbourn M, Bauer W. Investigation of cavitation and air entrainment during pilot injection in real-size multi-hole diesel nozzles. Fuel 263 (2020).
[9] Balz R, von Rotz B, Sedarsky D. In-nozzle flow and spray characteristics of large two-stroke marine diesel fuel injectors. Appl Therm Eng 2020;180.
[10] Kim B, Park S. Study on in-nozzle flow and spray behavior characteristics under various needle positions and length-to-width ratios of nozzle orifice using a transparent acrylic nozzle. Int J Heat Mass Transf 2019;143.
[11] Yang S, Ma Z, Li X, Hung DLS, Xu M. A review on the experimental non-intrusive investigation of fuel injector phase changing flow. Fuel 2020;259.
[12] Andriotis A, Gavaises M, Arcoumanis C. Vortex flow and cavitation in diesel injector nozzles. J Fluid Mech 2008;610.
[13] Hult J, Simmank P, Matlok S, Mayer S, Falgout Z, Linne M. Interior flow and near-nozzle spray development in a marine-engine diesel fuel injector. Exp Fluids 2016; 57.
[14] Payri R, Salvador FJ, Martí-Aldaraví P, Vaquerizo D. ECN Spray G external spray visualization and spray collapse description through penetration and morphology analysis. Appl Therm Eng 2017;112.
[15] Tang C, Feng Z, Zhan C, Ma W, Huang Z. Experimental study on the effect of injector nozzle K factor on the spray characteristics in a constant volume chamber: Near nozzle spray initiation, the macroscopic and the droplet statistics. Fuel 2017; 202.
[16] Taskiran OO. Investigation of the effect of nozzle inlet rounding on diesel spray formation and combustion. Fuel 2018;217.
[17] Lešnik L, Kegl B, Bombek G, Hočevar M, Biluš I. The influence of in-nozzle cavitation on flow characteristics and spray break-up. Fuel 2018;222.
[18] Zhang Z, Zhang W, Ma X, Awad OI, Xu H, Shuai S. Effects of GDI injector deposits on spray and combustion characteristics under different injection conditions. Fuel 2020;278.
[19] Zhang W, Li X, Huang L, Feng M. Experimental study on spray and evaporation characteristics of diesel-fueled marine engine conditions based on optical diagnostic technology. Fuel 2019;246.
[20] Xia J, Huang Z, Xu L, Ju D, Lu X. Experimental study on spray and atomization characteristics under subcritical, transcritical and supercritical conditions of marine diesel engine. Energy Convers Manage 2019;195.
[21] Xia J, Huang Z, Zhang L, Zhang Q, Zheng L, Liu R, Ju D, Lu X. Experimental comparisons on injection and atomization characteristics of diesel and its six-component surrogate under different critical conditions of marine engine. Energy Convers Manage 2020;205.
[22] Hult J, Matamis A, Baudoin E, Mayer S, Richter M. Spatiotemporal flame mapping in a large-bore marine diesel engine using multiple high-speed cameras. Int J Engine Res 2020;21.
[23] Herrmann K. Development of a reference experiment for large diesel engine combustion system optimization. In: CIMAC Congress 2007, Vienna, Austria.
[24] Herrmann K, von Rotz B, Schulz R, Weisser G, Schneider B, Boulouchos K. A spray combustion chamber facility for investigations in relation to large 2-stroke marine diesel engine combustion system optimization. In: Proceedings of the International Symposium on Marine Engineering (ISME), Kobe, Japan.
[25] Falgout Z, Linne M. Novel design for transparent high-pressure fuel injector nozzles. Rev Sci Instrum 2016;87.
[26] Balz R, Sedarsky D. Temperature Dependent In-Nozzle Flow Investigations of Marine Diesel Injectors. In: ILASS – Americas, 30th Annual Conference on Liquid Atomization and Spray Systems, Tempe, AZ, USA; 2019.
[27] Lei Y, Liu J, Qiu T, Mi J, Liu X, Zhao N, Peng G. Effect of injection dynamic behavior on fuel spray penetration of common-rail injector. Energy 2019;188.
[28] Gonzalez RC, Woods RE, Eddins SL. Digital Image Processing Using MATLAB. New Jersey: Pearson Prentice Hall; 2004.
[29] Hiroyasu H, Arai M. Structures of Fuel Sprays in Diesel Engines. SAE Technical Papers 1990;900475.
[30] Pang KM, Jangi M, Bai XS, Schramm J, Walther JH. Effects of Nozzle Diameter on Diesel Spray Flames: A numerical study using an Eulerian Stochastic Field Method. Energy Procedia 2017;142.
[31] Algayyim SJM, Wandel AP, Yusaf T. The impact of injector hole diameter on spray behaviour for butanol-diesel blends. Energies 2018;11.
[32] Gao Y, Wei M, Yan F, Chen L, Li G, Feng L. Effects of cavitation flow and stagnant bubbles on the initial temporal evolution of diesel spray. Exp Thermal Fluid Sci 2017;87.
[33] Abdullah MFE, Shinobu A, Tomoki K, Aizawa T. Effects of inversed-delta injection rate shaping on diesel spray flame liquid length, lift-off length and soot onset. Fuel 2019;258.
[34] Geng L, Wang Y, Wang Y, Li H. Effect of the injection pressure and orifice diameter on the spray characteristics of biodiesel. J Traffic Transp Eng 2020;7.
[35] Faeth GM. Structure and atomization properties of dense turbulent sprays. Symp (Int) Combust 1991;23.
[36] Faeth GM. Spray combustion phenomena. Symp (Int) Combust 1996;26.
[37] Lee K, Aalburg C, Diez FJ, Faeth GM, Sallam KA. Primary breakup of turbulent round liquid jets in uniform crossflows. AIAA J 2007;45.
[38] Medina M, Zhou Y, Fatouraie M, Wooldridge M. High-Speed Imaging Study on the Effects of Internal Geometry on High-Pressure Gasoline Sprays, SAE Technical Papers 2020-01-2111; 2020.
[39] Tang Y, Lou D, Wang C, Tan P, Hu Z, Zhang Y, Fang L. Study of visualization experiment on the influence of injector nozzle diameter on diesel engine spray ignition and combustion characteristics. Energies 2020;13.